Diagn Interv Radiol 2014; 20:34–41

CHEST IMAGING
ORIGINAL ARTICLE

Ultrashort echo time MRI of pulmonary water content: assessment in a sponge phantom at 1.5 and 3.0 Tesla

Francesco Molinari, Ananth J. Madhuranthakam, Robert Lenkinski, Alexander A. Bankier

PURPOSE
We aimed to develop a predictive model for lung water content using ultrashort echo time (UTE) magnetic resonance imaging (MRI) and a sponge phantom.

MATERIALS AND METHODS
Image quality was preliminarily optimized, and the signal-to-noise ratio (SNR) of UTE was compared with that obtained from a three-dimensional fast gradient echo (FGRE) sequence. Four predetermined volumes of water (3.5, 3.0, 2.5, and 2.0 mL) were soaked in cellulose foam sponges 1.8 cm^3 in size and were imaged with UTE-MRI at 1.5 and 3.0 Tesla (T). A multiple echo time experiment (range, 0.1–9.6 ms) was conducted, and the T2 signal decay curve was determined at each volume of water. A three-parameter equation was fitted to the measured signal, allowing for the calculation of proton density and T2*. The calculation error of proton density was determined as a function of echo time. The constants that allowed for the determination of unknown volumes of water from the measured proton density were calculated using linear regression.

RESULTS
UTE-MRI provided excellent image quality for the four phantoms and showed a higher SNR, compared to that of FGRE. Proton density decreased proportionally with the decreases in both lung water and field strength (from 3.5 to 2.0 mL; proton density range at 1.5 T, 30.5–17.3; at 3.0 T, 84.2–41.5). Minimum echo time less than 0.6 ms at 1.5 T and 1 ms at 3.0 T maintained calculation errors for proton density within the range of 0%–10%. The slopes of the lines for determining the unknown volumes of water with UTE-MRI were 0.12±0.003 at 1.5 T and 0.05±0.002 at 3.0 T ($P < 0.0001$).

CONCLUSION
In a sponge phantom imaged at 1.5 and 3.0 T, unknown volumes of water can be predicted with high accuracy using UTE-MRI.

From the Department of Radiology (F.M. ✉ *francescomolinari.dr@gmail.com*, R.L., A.A.B.), Beth Israel Deaconess Medical Center and Harvard Medical School, Boston, Massachusetts, USA; Global Applied Science Laboratory (A.J.M.), GE Healthcare, Boston, Massachusetts, USA.

Received 26 May 2013; revision requested 8 June 2013; revision received 15 June 2013; accepted 24 June 2013.

Published online 4 December 2013.
DOI 10.5152/dir.2013.13232

The volume of extravascular lung water increases in response to a variety of cardiac and respiratory injuries (1). In pulmonary edema of cardiac origin, the volume of water in the interstitial and alveolar compartments is related to the degree of cardio-pulmonary dysfunction (1). In acute lung injury occurring in septic or burn shock and in other critically ill patients, increased extravascular water overloads the pulmonary weight. The resulting multifocal collapse in the dependent regions of the lung rapidly reduces the alveolar-capillary gas exchange (2). A stress failure of the pulmonary capillaries leading to pulmonary edema also occurs after exposure to toxic or highly noxious infectious agents (3). In addition to lung injury and respiratory distress syndrome, pulmonary edema due to altered fluid dynamics or vascular permeability manifests in postsurgical lung (4) and renal disease (5). In acute events of pulmonary edema, the lung water content is a marker of the severity of the disease and must be promptly quantified to guide fluid therapy and ventilator strategies (6). In chronic disorders, the volume of interstitial water reflects the activity of the infiltrative process, and this volume decreases after the administration of antifibrotic drugs (7).

High-resolution computed tomography (HRCT) is the standard imaging technique for assessing lung anatomy. In addition, HRCT can suggest increased extracellular water in areas of the lung that appear as ground-glass opacities. Unfortunately, HRCT examinations are associated with an absorbed dose of ionizing radiation, which is of particular concern in young subjects and in longitudinal studies (8). A diagnostic method that could measure regional lung water without radiation exposure would have the potential to monitor noninvasively the progression of the disease and its response to therapy.

Lung water content can be determined using ^1H magnetic resonance imaging (MRI) (9–11). Because most of the lung tissue consists of water, the peak amplitude of the magnetic resonance (MR) signal obtained following the excitation pulse reflects the concentration of water protons (9). Unfortunately, conventional MR sequences have difficulties in measuring lung signal because of the rather long echo times (TEs) of these sequences, compared to the short T2* of lung water. Therefore, previous attempts at measuring lung water by MRI potentially underestimated the true water content by up to 40% (10). Half radiofrequency excitations and subsequent radial mapping from the center of the k-space have enabled TEs of approximately 0.1 ms, which are sufficiently short to detect the peak amplitude of the signal that determines the true proton density (12–18).

We hypothesized that ultrashort TE (UTE) MRI could provide reliable estimates of proton density and thus normative data for the analysis

of unknown water content in a sponge phantom. Therefore, the aim of this study was to develop a predictive model for lung water content using UTE-MRI and a sponge phantom.

Materials and methods

Study design

The first part of our study was performed to investigate the feasibility of UTE-MRI in a sponge phantom. The image quality was optimized, and the signal-to-noise ratio (SNR) was assessed in comparison with a fast gradient echo (FGRE) technique. In the second part of the study, the optimized imaging parameters were applied in a quantitative multiple-TE experiment aimed to model the proton density and T2* of the sponge phantom. Proton density was used to establish a normative model for the prediction of water content. Ethics committee approval was not required for this phantom experiment.

Sponge phantom

A rectangular cellulose foam sponge was used as a phantom model of the lung for the MR experiments. The sponge was freeze-dried and cut in four cubic samples of 1.8 cm^3 in size. The four cubic samples were isolated with plastic paper on their lateral perimeters and were lined on a rectangular rubber plate with an average spacing between the sponges of 2 mm. Preliminary imaging of the sponges showed that they produced no MR signal when dry. Before the start of the experiments, the four sponges were soaked with predetermined volumes of water (3.5, 3.0, 2.5, and 2.0 mL) using a syringe. The four volumes were selected to produce different densities of water without leaking from the sponges.

MRI experiments

The behavior of MR signal in the lung is known to depend on the magnetic field strength (19). Therefore, to assess more comprehensively the signal of the sponges soaked with water, we performed all the phantom experiments on a 1.5 and 3.0 Tesla (T) whole-body clinical MRI system (Excite HDxt, GE Healthcare, Milwaukee, Wisconsin, USA), offering maximum gradient strengths and slew rates of 33 mT/m and 120 T/m/s at 1.5 T and 40 mT/m and 150 T/m/s at 3.0 T, respectively. Two custom-made radiofrequency quadrature birdcage T/R coils were used for these studies. The bore diameter for both coils was 5×5 cm. The bore length was 6.5 cm for the coil used on the 1.5 T scanner and 12 cm for that used on the 3.0 T scanner. For all the experiments, the phantoms were positioned at the center of the radiofrequency coil. All the imaging parameters were identical for the experiments at 1.5 and 3.0 T. To assess sponge phantoms with very short TEs, a UTE pulse sequence with a radial k-space acquisition scheme was used (12). Because data acquisition immediately followed the radiofrequency excitation, radial sampling with UTE enabled TEs as short as 0.1 ms. The radial k-space was reconstructed online using a custom-built regridding algorithm. The gridded data were then Fourier transformed and were normalized to compensate for the nonideal sampling function (20).

MR experiments for image quality optimization

Twenty coronal images of the sponges were acquired on the 1.5 and 3.0 T MR systems, using the following parameters: repetition time (TR), 275 ms; TE, 0.1 ms; flip angle, 20°; slice thickness, 1 mm; slice spacing, 0 mm; acquisition matrix size, 512×499; field of view, 10×10 cm; in-plane resolution, 0.2×0.2 mm^2; interleaved multislice acquisition; pixel bandwidth, 244.1 Hz; number of averages, 2; and acquisition time, 4 min 45 s. Twenty comparative images with the same slice thickness were obtained using a three-dimensional FGRE sequence, with the following parameters: TR, 11 ms; TE, 2.1 ms; flip angle, 20°; acquisition matrix size, 384×384; field of view, 10×10 cm; in-plane resolution, 0.26×0.26 mm^2; interleaved multislice acquisition; pixel bandwidth, 244.1 Hz; number of averages, 2; and acquisition time, 2 min 15 s.

MR experiments for quantitative analysis

For the second set of experiments at 1.5 and 3.0 T, the UTE measurements were repeated on four coronal planes using a section thickness of 2 mm and TEs of 0.1, 0.2, 0.4, 0.8, 1.2, 1.6, 2.4, 3.2, 6.4, and 9.6 ms. The TE values were determined before the experiment by graphically simulating a T2* signal decay and then spacing the data points in the TE range on the exponential shape of the curve. No other imaging parameters of the sequence were changed. To monitor the progressive signal decay during the experiment, four samples of a gadolinium-based contrast agent (gadopentetate dimeglumine, Magnevist, Bayer Healthcare Pharmaceuticals Inc., Wayne, New Jersey, USA) were located next to the sponges. The four samples were obtained by diluting the gadolinium contrast solution with water, from 0.5 mol/L to concentrations of 250, 100, 50, and 25 mmol/L.

Image analysis

All the MRI experiments were analyzed using an open-source software package (Osirix®, version 3.9.2), on a Macintosh platform running the MacOS X operating system (version 10.6.8). An operator with nine years of experience in image analysis (F.M.) displayed the MR images on orthogonal planes and performed three-dimensional reconstructions for visual assessment. Subsequently, the operator selected the regions of interest (ROIs, 44×44 pixels) in the center of each sponge and in air for signal and noise measurements, respectively. To minimize the technical variability of the measurements, the size and position of the ROIs, among the images obtained at different section levels, and the two field strengths remained constant. All the ROIs were saved and used for quantitative analysis.

Statistical analysis

To predict water content in the phantom, a quantitative analysis of ROI data was developed in three steps. First, we calculated the SNR, proton density, and T2* of the sponges. Second, we determined the minimum TE to obtain reliable values for proton density. Third, we computed the parameters of the regression line, allowing for the calculation of unknown contents of water from proton density. Preliminary analysis of the pixel values in the ROIs resulted in a non-normal distribution of signal intensity

(Kolmogorov-Smirnov test; $P < 0.01$), which reflected the highly inhomogeneous nature of the sponge phantoms, as well as that of *in vivo* lung tissue. Therefore, summary statistics of signal data are expressed as medians with interquartile ranges (25%–75%) (21). Statistical analyses were performed using commercial software (Prism, version 5.0, GraphPad Software Inc., San Diego, California, USA). For all the tests, $P < 0.05$ indicated statistically significant differences.

Signal-to-noise ratio of UTE in comparison with the FGRE technique

The signal intensity of the sponges divided by the standard deviation of noise was expressed as the SNR. The SNR of the sponges from the UTE images at 0.1 ms was compared with that from the FGRE images using repeated-measures analysis of variance (ANOVA), followed by posthoc pairwise tests.

Proton density and T2 with UTE*

The proton density and T2* of the sponge phantom were calculated from a three-parameter fit to the measured signal, according to the exponential equation [1]:

$$SI=PD\times e^{(-TE/T2^*)}+N$$

where SI is measured signal intensity, PD is proton density, and N includes background noise (22). The same fitting analysis performed pixel-wise produced parametric maps of proton density and T2*. As part of the regression analysis, vertical distances of the data from the ideal curve (residuals) were minimized using the sum of squares method (23). As an estimate of the goodness of the fit, we considered the plausibility of the best-fit parameter values with their confidence intervals, root mean squares (Sy.x), and coefficients of determination (R^2). Statistically significant deviation of measured data from the theoretical model of the exponential equation was also assessed by a Runs test. Finally, the model was validated against the asymmetry of the source signal values by assessing the normality of the distribution of the residuals (23).

Minimum TE to calculate proton density

The minimum TE that allows for consistent assessment of proton density was determined by calculating the fractional error of the proton density. The regression curve, starting from the minimum TE of 0.1 ms and ending at the maximum TE of 9.6 ms, provided the reference value of proton density. Other regression curves were obtained by progressively increasing the minimum TE (0.2, 0.4, 0.8, etc.) while maintaining the fixed maximum TE of 9.6 ms. Values of proton density calculated from reduced data points were subtracted from the reference proton density and were expressed as a percentage of the reference (fractional error) (24). The fractional error of proton density was plotted against TE.

Normative model for the prediction of water content

Reference values of proton density were plotted against the known volumes of water in the four sponges. A regression line was calculated to obtain the slope of the line that allows for the determination of unknown volumes of water from measured proton densities. A 0 value was allowed for the intercepts. Statistical analysis for this linear model consisted of calculation of Sy.x and the possibility of zero values for the slope using the Runs test. The slopes are expressed with 95% confidence intervals. To test the consistency of the analysis, we also performed linear regression between the volume of water and T2* values.

Results

Image quality optimization

The three-dimensional representation of a sponge by UTE at 1.5 T and representative images of the sponges obtained at 3.0 T by UTE and FGRE sequences are presented in Figs. 1 and 2, respectively.

Signal-to-noise ratio of UTE in comparison with FGRE technique

Fig. 3 shows the SNR values of the sponges. The overall SNR was significantly higher at 3.0 T than at 1.5 T ($P < 0.001$; ANOVA). The difference was also significant by pairwise comparisons (UTE at 3.0 vs. 1.5 T, and FGRE at 3.0 vs. 1.5 T; $P < 0.001$; posthoc analysis). At both 1.5 and 3.0 T, the SNRs of all four sponges were significantly higher on the UTE images than on the FGRE images ($P < 0.001$; Fig. 3).

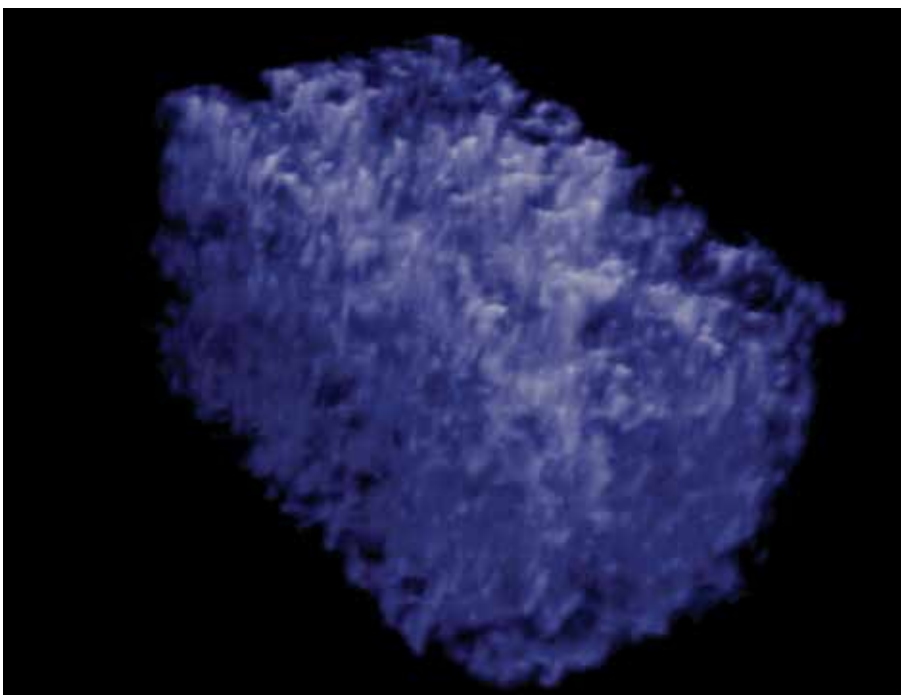

Figure 1. Three-dimensional maximum intensity projection of a sponge with ultrashort echo time (UTE). The lung phantom model was obtained from 20 coronal UTE images at TE of 0.1 ms. The voxel dimension was 0.19×0.2×1 mm^3. The sponge was soaked with 2.5 mL of water.

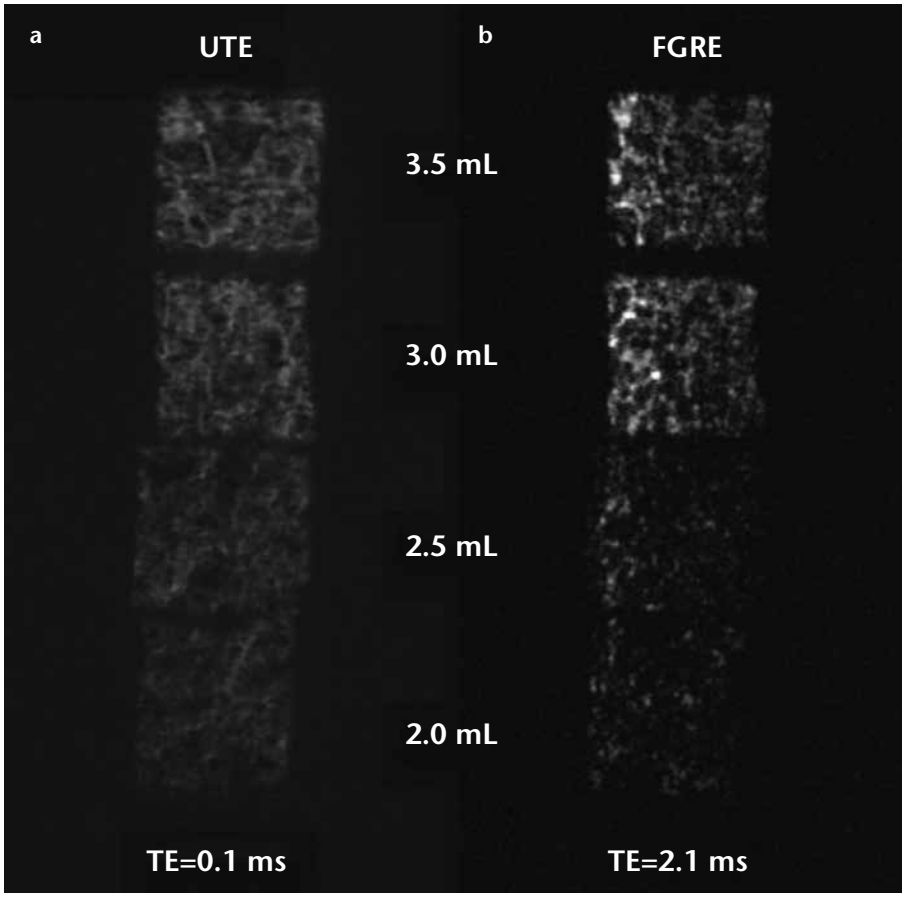

Figure 2. a, b. Sponge phantoms imaged at 3.0 T using ultrashort echo time (UTE) **(a)** and fast gradient echo (FGRE) **(b)** techniques. From top to bottom, four sponges, 1.8 cm^3 in size, were soaked with 3.5, 3.0, 2.5, and 2.0 mL of water. The TE was 0.1 ms for the UTE sequence and 2.1 ms for the FGRE sequence. All four sponges were perfectly represented by UTE. Using FGRE, the sponges containing 3.5 and 3.0 mL of water were visible, although the image details were limited. At 2.5 and 2.0 mL, the FGRE technique produced a remarkably low signal, and the structure of the sponge was almost completely undetectable. Conversely, even at the minimum volume of water of 2.0 mL, the UTE sequence showed fine details of the alveolar structure of the sponge, and the noise level appeared visibly reduced.

Proton density and T2 with UTE*

Fig. 4 shows the sponge phantoms imaged with multiple TEs at 3.0 T. Fig. 5 demonstrates the signal decay of the sponges at 1.5 and 3.0 T. The four sponges showed higher signals at 3.0 T than at 1.5 T. The signal decay at 3.0 T was very rapid (slopes of the curves in Fig. 5). The signal difference at 1.5 T was almost exclusively visible in the TE range of 0.1–3.2 ms. The Sy.x and R^2 values, determined from the nonlinear regression analysis, ranged from 2.01 to 0.36 and from 0.999 to 0.982, respectively. The Runs test confirmed that no significant deviations from the model existed (range of *P* values, 0.167–0.405). Normality of the distribution of residuals was demonstrated ($P > 0.10$), confirming that the model was robust against the asymmetry of the source signal values. At 3.0 T, the values of proton density (±95% confidence interval, CI) for the four sponges at 3.5, 3.0, 2.5, and 2.0 mL of water were 84.2±4.5, 60.6±3, 48.4±3.5, and 41.5±5.3, respectively; the values of T2* (±95% CI) were 1.41±0.18, 1.37±0.17, 1.29±0.25, and 0.94±0.13 ms, respectively. At 1.5 T, the values of proton density (±95% CI) for the four sponges were 30.5±0.9, 26.4±2.3, 19.5±1.9, and 17.3±2; the values of T2* (±95% CI) were 2.56±0.18, 2.13±0.51, 2.01±0.53, and 1.59±0.49 ms. Fig. 6 shows the parametric maps of the proton density and T2* values.

Minimum TE to calculate proton density

Fig. 7 shows the relationship between the fractional error of proton density and the minimum TE for the calculation of proton density. At 3.0 T, minimum TEs of up to 1 ms might result in calculation errors within the range of 0%–10%. The fractional error of proton density increases dramatically with minimum TEs greater than 1 ms and reaches a plateau of 55%–60% at TEs greater than 3.6 ms. At 1.5 T, a fractional error of 10% is reached at a minimum TE of 0.6 ms, and the plateau of 36%–40% starts at a minimum TE of 1.6 ms.

Normative model for the prediction of water content

Fig. 8 shows the regression lines between the values of proton density calculated by UTE and the corresponding volumes of water. At both 1.5 and 3.0 T, the regression analysis was statistically validated (R^2=0.947 at 1.5 T, R^2=0.786 at 3.0 T; very small Sy.x range, 0.15–0.29; no significant deviations from linearity; range of *P* values, 1.0–0.5). The slopes of the lines allowing for the prediction of unknown volumes of water from the calculated values of proton densities were significantly different from 0 ($P < 0.0001$). At 1.5 T, the slope of the line was 0.12±0.003 (95% CI, 5% of the slope). For example, using this multiplicative factor, a calculated value of proton density of 60 indicated a content of water in the range of 5.85–6.15 mL. At 3.0 T, the slope of the line was 0.05±0.002 (95% CI, 8% of the slope). Moreover, using this multiplicative factor, a calculated value of proton density of 60 indicated a water content of 2.88–3.12 mL.

Discussion

In this study, we showed that unknown volumes of water in sponge phantoms can be predicted using UTE-MRI. The prediction model, based on proton densities, provided reliable normative data for the analysis of water content in a lung parenchymal phantom.

The air content in the living lung results in a double limitation for MRI. First, air reduces the relative H-density of lung tissue, indicating that fewer water protons are available per unit of volume to produce transversal magnetization and to generate MR signal. Second, air in the alveolar units influences the magnetic behavior of the lung so that MR signal disappears in

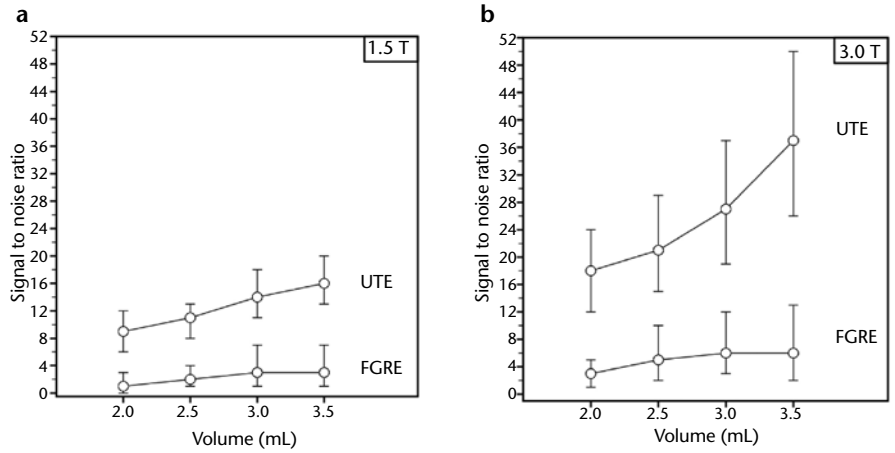

Figure 3. a, b. Signal-to-noise ratio (SNR) of the sponges at 1.5 T **(a)** and 3.0 T **(b)**. Data in the graph represent medians with interquartile ranges (25%–75%) of SNR of the phantoms calculated from ultrashort echo time (UTE) and fast gradient echo (FGRE) images of 1 mm in section thickness, with TE values of 0.1 and 2.1 ms, respectively. The SNR was higher using UTE than with FGRE at both 1.5 and 3.0 T.

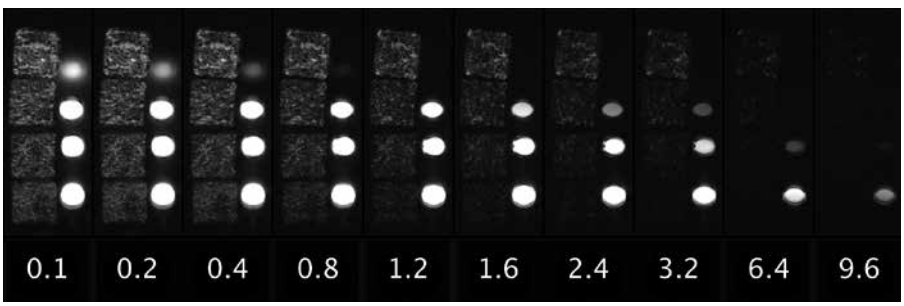

Figure 4. Sponges and gadolinium samples imaged at 3.0 T with progressive TEs. Numbers at the bottom of each frame indicate the TEs (ms) used in the experiment. From the top to bottom of each frame, the four sponges received 3.5, 3.0, 2.5, and 2.0 mL of water, and the four gadolinium samples were diluted at concentrations of 250, 100, 50, and 25 mmol/L. The gadolinium samples served as a homogeneous reference material for measuring signal decay during the experiment. Both the sponges and gadolinium samples showed progressive signal decay in the range of TEs of the experiment (0.1–9.6 ms). Within the TE range of 0.8–1.6 ms, the sponge retaining the smallest volume of water (2 mL) became progressively less visible. The gadolinium sample at the highest concentration (250 mmol/L, the uppermost in each frame) experienced very fast signal decay and was not visible at a TE greater than 0.8 ms.

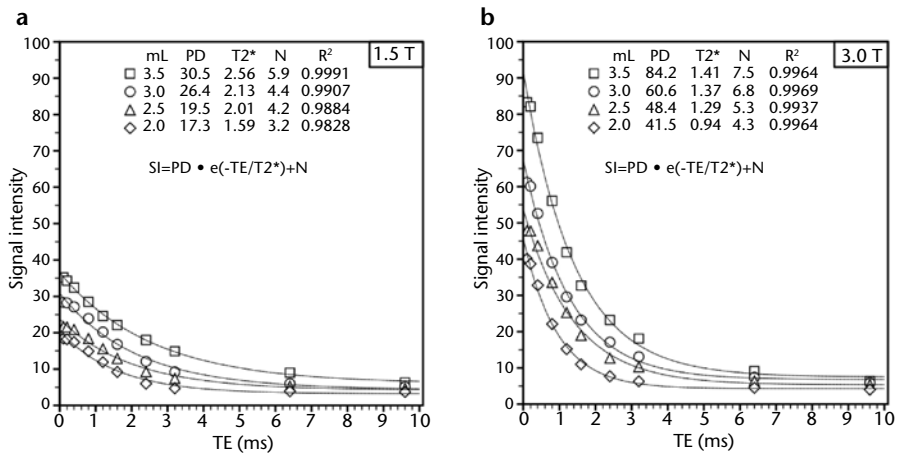

Figure 5. a, b. Signal decay curves of the sponges at 1.5 T **(a)** and 3.0 T **(b)**. Data points in the plots represent the values of signal intensity measured from the regions of interest of the sponges at TEs of 0.1, 0.2, 0.4, 0.8, 1.2, 1.6, 2.4, 3.2, 6.4, and 9.6 ms. Lines represent the fits of the exponential equation. The three parameters of the fitting equation are proton density (PD), T2*, and background noise (N). R^2 values of the fitting are also reported.

less than 1 ms (9). Despite these limitations, lung MRI can be used clinically to visualize parenchymal diseases, particularly those that increase proton density (consolidations, tumors, etc.) (19, 25). Diffuse alterations that do not sufficiently increase the water density of the organ (interstitial pulmonary edema or mild chronic infiltrative disease) or decrease it (emphysema) are underdetected by conventional MR techniques. As virtually all the signal measured in the lung derives from water protons, the possibility of accurately predicting pulmonary water by MRI becomes clearly attractive for characterizing, staging and monitoring of pulmonary disease.

Sponge phantoms have been previously used to simulate the alveolar structure of the lung (26) and to perform MR signal measurements (27). The porous structure of the dry sponge produces a negligible MR signal. The known volumes of water added to the sponges were well absorbed, which produced an appropriate setting for signal measurements (27).

Since UTE-MRI of the lung was first demonstrated in the early 1990s on a 1.5 T system (28), most of the subsequent studies have been performed on animal MR systems at higher field strengths (14, 15, 18, 22). Only recently, investigators performed UTE-MRI of the lung in animal models using clinical systems at 3.0 T (16, 17). However, the combined feasibility of visualization and quantitative analysis of lung water content using UTE-MRI at both 1.5 and 3.0 T have been under-reported. We conducted our experiments on human MRI units. The coil size was adapted to maximize the signal reception from the small, water-soaked sponges. The UTE sequence was set up identically at 1.5 and 3.0 T.

Imaging was performed using a projection acquisition approach, with half radiofrequency excitations and subsequent radial mapping from the center of the k-space. The sequence minimizes the delay between the end point of the excitation pulse and the data sampling, which allows for a reduction of the TE below the limit of clinical detectability provided by conventional gradient echo techniques (1–2 ms)

(12). The minimal TE allowed in our experiments was 0.1 ms, which was identical to the most recent UTE-MRI studies (16, 17). The advantage of such a short TE is the gaining of sensitivity over the rapid signal loss that limits both qualitative and quantitative MRI of lung parenchyma.

Low SNR and blurring from biological motion can degrade image quality on lung MRI. In the static setting of our experiments, we selectively addressed the low SNR issue as a limiting factor for image quality. The UTE images were compared with the FGRE images, in which FGRE represents the reference clinical method for high-resolution imaging of lung morphology. Using the typical acquisition parameters for clinical imaging (matrix size of 384×384), FGRE produced acceptable image quality, which was remarkably dependent on the water content in the sponge. This finding reflected clinical conditions well and confirmed the appropriateness of the sponge model as a surrogate for the imaging of lung parenchyma. Conversely, UTE images provided excellent image quality, even at the lowest water content (2 mL). As the minimum TE with UTE was 20 times shorter than the minimum TE offered by the FGRE technique, the SNR provided by UTE was significantly increased at both 1.5 and 3.0 T. The extra signal gained using UTE allowed for an increase in image resolution (voxel size of 0.2×0.2×1 mm^2). Excellent three-dimensional reformations of the UTE images were obtained, even at the lower field strength (1.5 T, Fig. 1).

The UTE sequence offers the possibility of measuring signal at different TE intervals (16, 17, 22). Thus, signal decay can be observed empirically in the submillisecond time range, during which the majority of lung signal is believed to disappear at an extremely rapid rate. Our quantitative experiments confirmed the exponential decay of sponge phantom signal, for which the starting point of the curve (y intercept) represented proton density, and the shapes of which were modulated by the decay constant (T2*). T2* was shorter at 3.0 T than at 1.5 T, which inherently suggested an air/tissue interface effect similar to that observed in the alveoli (9). Additionally, the T2* of the sponge soaked with 2 mL of water was similar to the value reported at the same field strength in a previous animal study (0.9 ms), suggesting another similarity between our simulation and the lung tissue (17).

The fitting equation was adapted from the study of Olsson et al. (22). The monoexponential fit allowed for consistent calculation of the proton density and T2* of the sponges, and the goodness of the fit was confirmed statistically. This mathematical approach is justified when assuming that long T2 components are negligible. The assumption is reasonable in the lung because signal decay is primarily driven by the inhomogeneity of the magnetic field, which is created by the difference in the diamagnetic susceptibility between air and water (T2*). Additionally, long T2 components, which would suggest the use of a bi-exponential or multi-exponential fit, have been reported at longer TEs than those implemented in our experiment (12).

Following the analysis of the fitting parameters, we assessed the minimum value of TE that allows for consistent calculation of proton density. Previous studies using submillisecond MRI of the lung did not assess this important aspect of quantitative analysis. UTE-MRI provides for direct measurement of all transversal magnetization at the very beginning of the decay curve, so it can be considered the most precise method for assessing proton density. As the water content is predicted with regression analysis, errors in the calculation of proton density inevitably result in inaccurate estimates of the volume of water. We evaluated the behavior of the fractional error of proton density by simulating the fitting of curves with minimum TEs progressively shifted toward higher values. At 3.0 T, a minimum TE of 1 ms resulted in a 10% calculation error of proton density. At 1.5 T, the same error occurred at a minimum TE of 0.6 ms. This difference is easily explained, considering that the values of proton density calculated at 1.5 T were lower than those at 3.0 T, and the error becomes more relevant as the relative percentage of small proton density values grows.

Previous studies have investigated the possibility of noninvasively estimating lung water content using MRI. MR-derived parameters have been validated using gravimetric and morphometric measurements of lung water and lung tissue density, respectively, in animal models (9, 29). Because the MR techniques were not sufficiently sensitive to the rapid decay of lung signal (30), signal measurements were found to have underestimated the lung water content by up to 40% (9, 10). Multi-echo gradient echo sequences were also evaluated for the quantitative imaging of lung water and density in animals (11) and in healthy subjects (31, 32). UTE-MRI is intrinsically more sensitive to the rapid decay of lung signal than gradient echo sequences, thus offering the opportunity to estimate lung water precisely (16). In our study, the prediction model was determined by calculating the regression line between known volumes of water and proton densities. The fitting analysis was robust, and the confidence intervals of the proton density values were very small. The statistical variability around the calculated slopes was minimal, and the whole method of converting proton density into water content was very precise.

This study has limitations. The sponge phantoms approximated the complex architecture of the lung. However, in living lungs, the blood and dry tissue have non-negligible weights, which vary according to the body mass index and can contribute to the total proton density. In addition, in living lungs, lung water is separated in the extravascular and vascular compartments. Our sponges also provided a model of rather uniformly distributed T2*, neglecting the effects of gravity. In reality, water can accumulate in a lung region and decrease the susceptibility effect of the air-tissue interface, resulting in a long local T2*. Similarly, if air exceeds water, the local T2* decreases. The static nature of our experiments allowed for the removal of sources of signal loss and image quality degradation (i.e., respiratory and cardiac motion). The model did not account for the behavior of the lung at different volumes and with flowing intravascular blood. Cutillo et al. (9) reported that water density was inversely correlated with lung volume. Consistent with this relationship, they

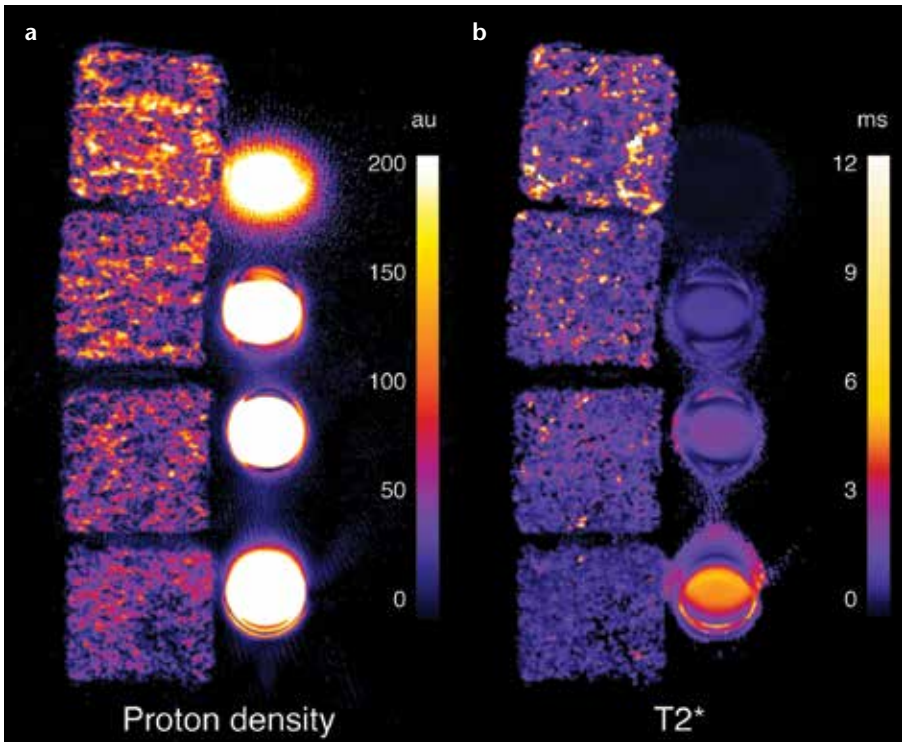

Figure 6. a, b. Proton density and T2* maps at 3.0 T. Proton density **(a)** decreases proportionally with the water content in the four sponges. The T2* of the sponges **(b)** was shorter in the sponge soaked with 2 mL of water *(bottom)* and increased progressively in the sponges in larger volumes of water *(top)*. The gadolinium sample at higher concentration (first in line from the top) showed a visible artifact due to the extremely short T2* time.

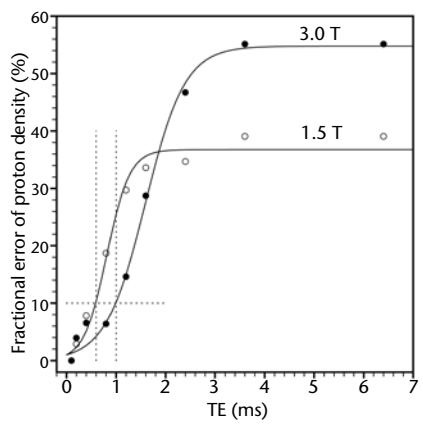

Figure 7. Fractional error of proton density. Data in the plot represent the fractional errors of proton density from the four sponges. The minimum TE to avoid substantial calculation errors of proton density was 1 ms at 3.0 T and 0.6 ms at 1.5 T.

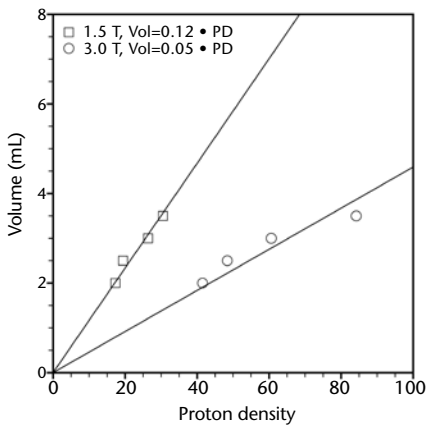

Figure 8. Normative model for the prediction of water content. Data in the graph indicate the values of proton densities calculated using ultrashort echo time and the corresponding volumes of water in the sponges. From the scale constant of the regression lines, unknown volumes of water could be predicted. The prediction was more accurate on the 3.0 T scale as the range of values of proton density was wider (45.8–91.7 at 3.0 T vs. 19.5–36.4 at 1.5 T).

concluded that water density increases substantially only when lung inflation is remarkably reduced (e.g., collapse). This condition was not induced in our sponge phantom. Because we used UTE-MRI, the half radiofrequency pulse might also have produced artifacts with flowing blood. MR technical factors (coil sensitivity, voxel size, TR, etc.) can also influence the linear relationship between the measured signal and the estimated water content. Although the technical parameters were not changed in the experiments, the TR values were sufficiently short to allow a T1 contribution to the signal. Difficulties in translating the phantom experiment to living lungs also include the small coils used in this study. Human body-size coils have generally lower SNRs and less uniform fields. The coils also differed between the 1.5 and 3.0 T experiments. The TR and pixel size between the FGRE and UTE sequences varied. Both factors might have influenced the results in the SNR comparisons. For all these reasons, the results of our study should be further validated in living lungs.

In conclusion, in a sponge phantom imaged at 1.5 and 3.0 T, unknown volumes of water can be predicted with high accuracy using UTE-MRI.

Conflict of interest disclosure

The authors declared no conflicts of interest.

References

1. Murray JF. Pulmonary edema: pathophysiology and diagnosis. Int J Tuberc Lung Dis 2011; 15:155–160.
2. Guerin C, Debord S, Leray V, et al. Efficacy and safety of recruitment maneuvers in acute respiratory distress syndrome. Ann Intensive Care 2011; 1:9. [CrossRef]
3. West JB, Tsukimoto K, Mathieu-Costello O, Prediletto R. Stress failure in pulmonary capillaries. J Appl Physiol 1991; 70:1731–1742.
4. Miserocchi G, Beretta E, Rivolta I. Respiratory mechanics and fluid dynamics after lung resection surgery. Thorac Surg Clin 2010; 20:345–357. [CrossRef]
5. Basu RK, Wheeler D. Effects of ischemic acute kidney injury on lung water balance: nephrogenic pulmonary edema? Pulm Med 2011; 2011:414253.
6. Camporota L, De Neef M, Beale R. Extravascular lung water in acute respiratory distress syndrome: potential clinical value, assumptions and limitations. Crit Care 2012; 16:114. [CrossRef]
7. Samah M, El-Aidy AE, Tawfik MK, Ewais MM. Evaluation of the antifibrotic effect of fenofibrate and rosiglitazone on bleomycin-induced pulmonary fibrosis in rats. Eur J Pharmacol 2012; 15:186–193. [CrossRef]
8. Molinari F, Tack DM, Boiselle PM, et al. Radiation dose management in thoracic CT: an international survey. Diagn Interv Radiol 2013; 19:201–209.

9. Cutillo AG, Goodrich KC, Ganesan K, et al. Lung water measurement by nuclear magnetic resonance: correlation with morphometry. J Appl Physiol 1995; 79:2163–2168.
10. Lange NR, Schuster DP. The measurement of lung water. Crit Care 1999; 3:R19–R24. [CrossRef]
11. Holverda S, Theilmann RJ, Sa RC, et al. Measuring lung water: ex vivo validation of multi-image gradient echo MRI. J Magn Reson Imaging 2011; 34:220–224. [CrossRef]
12. Robson MD, Bydder GM. Clinical ultrashort echo time imaging of bone and other connective tissues. NMR Biomed 2006; 19:765–780. [CrossRef]
13. Bergin CJ, Noll DC, Pauly JM, Glover GH, Macovski A. MR imaging of lung parenchyma: a solution to susceptibility. Radiology 1992; 183:673–676.
14. Gewalt SL, Glover GH, Hedlund LW, Cofer GP, MacFall JR, Johnson GA. MR microscopy of the rat lung using projection reconstruction. Magn Reson Med 1993; 29:99–106. [CrossRef]
15. Kuethe DO, Adolphi NL, Fukushima E. Short data-acquisition times improve projection images of lung tissue. Magn Reson Med 2007; 57:1058–1064. [CrossRef]
16. Takahashi M, Togao O, Obara M, et al. Ultra-short echo time (UTE) MR imaging of the lung: comparison between normal and emphysematous lungs in mutant mice. J Magn Reson Imaging 2010; 32:326–333. [CrossRef]
17. Togao O, Tsuji R, Ohno Y, Dimitrov I, Takahashi M. Ultrashort echo time (UTE) MRI of the lung: assessment of tissue density in the lung parenchyma. Magn Reson Med 2010; 64:1491–1498. [CrossRef]
18. Zurek M, Bessaad A, Cieslar K, Crémillieux Y. Validation of simple and robust protocols for high-resolution lung proton MRI in mice. Magn Reson Med 2010; 64:401–407.
19. Wielputz M, Kauczor HU. MRI of the lung: state of the art. Diagn Interv Radiol 2012; 18:344–353.
20. Pipe JG. Reconstructing MR images from undersampled data: data-weighting considerations. Magn Reson Med 2000; 43:867–875. [CrossRef]
21. Hill T, Lewicki P. STATISTICS methods and applications. Tulsa: StatSoft, 2007.
22. Olsson LE, Lindahl M, Onnervik P-O, et al. Measurement of MR signal and T2* in lung to characterize a tight skin mouse model of emphysema using single-point imaging. J Magn Reson Imaging 2007; 25:488–494. [CrossRef]
23. Bates DM, Watts DG. Nonlinear regression analysis and its applications. New York: John Wiley & Sons, 2007; 365.
24. Tzamaloukas AH, Jackson JE, Long DA. The fractional error as a means of assessing agreement between two methods measuring the same variable. Clin Chem 1987; 33:1944–1945.
25. Puderbach M, Hintze C, Ley S, Eichinger M, Kauczor H-U, Biederer J. MR imaging of the chest: a practical approach at 1.5T. Eur J Radiol 2007; 64:345–355. [CrossRef]
26. MacLennan FM, Foster MA, Smith FW, Crosher GA. Measurement of total lung water from nuclear magnetic resonance images. Br J Radiol 1986; 59:553–560. [CrossRef]
27. Menke J, Helms G, Larsen J. Viewing the effective k-space coverage of MR images: phantom experiments with fast Fourier transform. Magn Reson Imaging 2010; 28:87–94. [CrossRef]
28. Bergin CJ, Glover GH, Pauly JM. Lung parenchyma: magnetic susceptibility in MR imaging. Radiology 1991; 180:845–848.
29. Cutillo AG, Morris AH, Ailion DC, Durney CH, Case TA. Determination of lung water content and distribution by nuclear magnetic resonance imaging. J Thorac Imaging 1986; 1:39–51. [CrossRef]
30. Rhodes CG. Measurement of lung water using nuclear magnetic resonance imaging. Br J Radiol 1986; 59:1135–1136. [CrossRef]
31. Theilmann RJ, Arai TJ, Samiee A, et al. Quantitative MRI measurement of lung density must account for the change in T(2) (*) with lung inflation. J Magn Reson Imaging 2009; 30:527–534. [CrossRef]
32. Zhang Z Jr. Calculation of the normal range of extravascular lung water. Crit Care 2010; 14:448. [CrossRef]